Acta Pharmacologica Sinica

www.nature.com/aps

ARTICLE

Dysregulation of iron homeostasis by TfR-1 renders EZH2 wild type diffuse large B-cell lymphoma resistance to EZH2 inhibition

Lei Yu[1,2], Ya-fang Wang[1], Jian Xiao[1,2], Qian-qian Shen[1], Shuai-shuai Chi[1,2], Ying-lei Gao[1], Dong-ze Lin[1], Jian Ding[1,2,3,4]✉, Yan-fen Fang[1,2,3]✉ and Yi Chen[1,2,4,5]✉

EZH2 has been regarded as an efficient target for diffuse large B-cell lymphoma (DLBCL), but the clinical benefits of EZH2 inhibitors (EZH2i) are limited. To date, only EPZ-6438 has been approved by FDA for the treatment of follicular lymphoma and epithelioid sarcoma. We have discovered a novel EZH1/2 inhibitor HH2853 with a better antitumor effect than EPZ-6438 in preclinical studies. In this study we explored the molecular mechanism underlying the primary resistance to EZH2 inhibitors and sought for combination therapy strategy to overcome it. By analyzing EPZ-6438 and HH2853 response profiling, we found that EZH2 inhibition increased intracellular iron through upregulation of transferrin receptor 1 (TfR-1), ultimately triggered resistance to EZH2i in DLBCL cells. We demonstrated that H3K27ac gain by EZH2i enhanced c-Myc transcription, which contributed to TfR-1 overexpression in insensitive U-2932 and WILL-2 cells. On the other hand, EZH2i impaired the occurrence of ferroptosis by upregulating the heat shock protein family A (Hsp70) member 5 (HSPA5) and stabilizing glutathione peroxidase 4 (GPX4), a ferroptosis suppressor; co-treatment with ferroptosis inducer erastin effectively overrode the resistance of DLBCL to EZH2i in vitro and in vivo. Altogether, this study reveals iron-dependent resistance evoked by EZH2i in DLBCL cells, and suggests that combination with ferroptosis inducer may be a promising therapeutic strategy.

Keywords: diffuse large B-cell lymphoma; EZH2; TfR-1; GPX4; ferroptosis; HH2853

Acta Pharmacologica Sinica (2023) 44:2113–2124; https://doi.org/10.1038/s41401-023-01097-4

INTRODUCTION

Polycomb repressive complex 2 (PRC2) is a type of histone methylation transferase assembled by enhancer of zeste homolog 2 (EZH2), embryonic ectoderm development (EED), suppressor of zeste 12 (SUZ12), and the RbAp46/48 subunit [1]. EZH2, the crucial catalytic subunit of PRC2, induces trimethylation on the 27th lysine of histone H3 (H3K27) by transferring methyl groups from *S*-adenosyl-*L*-methionine, ultimately leading to gene silencing [1]. Many studies have interpreted the aberrant expression of PRC2 and/or EZH2 in a variety of human cancers [2]. Moreover, EZH2 has been shown to have multiple gain-of-function mutations that play pivotal roles in cancer development and progression [3]. Therefore, targeting EZH2 has been validated as a prospective therapeutic strategy for cancer treatment, and tremendous efforts have been made to develop EZH2 inhibitors, such as tazemetostat (EPZ-6438), GSK126. To date, only EPZ-6438 has been approved by the FDA for the treatment of follicular lymphoma and epithelioid sarcoma [4]. Several EZH2 inhibitors are currently undergoing clinical trials.

Although epigenetic modifiers have been considered as good targets for anti-tumor drugs for many years, their extensive biological effects and unclear mechanisms have led to limited success in drug development. The discovery of EZH2 inhibitors has been one of the few successes; however, EZH2 inhibitors still pose many challenges. EPZ-6438 and other EZH2 inhibitors have shown promising effects on only a few tumors in clinic [5, 6], with limited benefits and serious primary drug resistance [7]. Therefore, it is an urgent need to find more effective EZH2 inhibitors, and rational combination therapies to overcome primary resistance.

Recently, more attention has been paid to the role of iron in cellular biological processes, especially in the initiation and growth of tumors [8]. Compared to normal cells, a relatively high level of cellular iron is found in tumors, which accelerates cell proliferation, angiogenesis, and epigenetic remodeling [9]. Our previous work revealed that the histone methyltransferase G9a exerts its oncogenic function in breast cancer by repressing hephaestin transcription, encouraging iron accumulation [10]. In addition, some studies have reported the relationship between drug resistance and iron metabolism and the utilization of this knowledge for the reversal of drug resistance [11]. Emerging evidence suggests that ferroptosis, triggered by iron overload [12, 13], is related to drug resistance, and may represent a

[1]Division of Anti-Tumor Pharmacology, Shanghai Institute of Materia Medica, Chinese Academy of Sciences, Shanghai 201203, China; [2]University of Chinese Academy of Sciences, No.19A Yuquan Road, Beijing 100049, China; [3]State Key Laboratory of Drug Research, Shanghai Institute of Materia Medica, Chinese Academy of Sciences, Shanghai 201203, China; [4]Shandong Laboratory of Yantai Drug Discovery, Bohai Rim Advanced Research Institute for Drug Discovery, Yantai 264117, China and [5]State Key Laboratory of Chemical Biology, Shanghai Institute of Materia Medica, Chinese Academy of Sciences, Shanghai 201203, China
Correspondence: Jian Ding (jding@simm.ac.cn) or Yan-fen Fang (yffang@simm.ac.cn) or Yi Chen (ychen@simm.ac.cn)

Received: 31 January 2023 Accepted: 22 April 2023
Published online: 25 May 2023

therapeutic opportunity to prevent drug resistance [11, 14, 15]. Iron homeostasis also has been proved to be under epigenetic regulation, such as DNA methylation, histone modification, and post-transcriptional modification. These studies have received increasing attention, and may represent a therapeutic opportunity to overcome drug resistance.

The discovery and the preclinical characterizations of a novel, orally bioavailable dual inhibitor of EZH1/2, named HH2853, were disclosed by Haihe Biopharma and us [16], which currently is undergoing phase I clinical trials in the USA and China (NCT04390737, CTR20201548). It exhibited superior anti-tumor efficacy in several tumor xenograft models compared with FDA-approved EZH2 selective inhibitor EPZ-6438 at a comparable dose level. Nevertheless, HH2853 also shows weak anti-tumor activity against EZH2 wild type (EZH2-WT) DLBCL cells in vitro and in vivo. Thus, we attempted to explore the mechanism underlying the primary resistance to EZH2 inhibitors and seek for combination therapy strategy to overcome it. We found that dysregulation of iron homeostasis resulted from EZH2 inhibition might be associated with the primary resistance to EZH2-WT DLBCL.

MATERIALS AND METHODS

In vitro EZH1/EZH2 methyltransferases assay

The effects of EPZ-6438 and HH2853 on the activity of EZH2-WT, EZH2 Y641F, EZH2 A677G, EZH2 Y641C, EZH2 Y641N (EZH2/EED/SUZ12/RbAp48/ AEBP2), and EZH1 (EZH1/EED/SUZ12/RbAp48/AEBP2) were detected by HTRF assay (Cisbio, Codolet, France). In this assay, enzyme, SAM (Sigma, Darmstadt, Germany), compound and peptide substrate were added to the plate and incubated at room temperature for 4 h. Then, 10 μL antibody of Eu-H3K27me3 and SA-XL665 (Cisbio) was added into the plate. After incubation for 1 h at room temperature, signal was collected with an HTRF compatible reader (665 nm/620 nm).

Cell culture

Human DLBCL cell lines Pfeiffer, KARPAS-422, U-2932, and WILL-2 were obtained from the German Collection of Microorganisms and Cell Cultures (Braunschweig, Germany) or American Type Culture Collection (Virginia, USA), and OCI-LY10 was obtained from Cobioer (Nanjing, China).

Cell viability assay

Cell Counting Kit-8 (CCK-8, Life-iLab, shanghai, China) was used to measure cell viability according to the manufacturer's protocol. Briefly, cells were seeded in 96-well plates overnight and treated with indicated compounds for 6 days. Subsequently, CCK-8 was added to the medium and incubated at 37 °C for 2–4 h. The absorbance (optical density, OD) was measured at a wavelength of 450 nm.

Western blotting

Experiments were conducted as described previously [17]. Proteins probed by the following antibodies were used: anti-TfR-1(#13113 s, CST, Massachusetts, USA), anti-c-Myc (#18583, CST), anti-EED(#85322, CST), anti-EZH1 (#42088 s, CST), anti-EZH2 (#5246, CST), anti-HSPA5 (#3177 s, CST), anti-Ubiquitin (#43124 s, CST), anti-β-Actin (60008-1-Ig, Proteintech, Illinois, USA), anti-Histone H3K27me3 (17168-1-AP, Proteintech), anti-GAPDH (60004-1-Ig, Proteintech), anti-FSP1 (A12128, Abclone, Wuhan, China), anti-DHODH (A6899, Abclone), anti-GPX4 (A11243, Abclone), anti-α-tubulin (AC012, Abclone) and anti-Histone H3K27ac (#39685, Active motif, California, USA).

Co-immunoprecipitation analysis (Co-IP)

Sample proteins were incubated with GPX4 (A11243, Abclonal), HSPA5 (#3177, CST), or normal rabbit IgG (#2729, CST) overnight at 4 °C with gentle shaking. Then, they were incubated with Protein A/G Magnetic Beads (Thermo Fisher Scientific) for 4 h at 4 °C and the change was detected by Western blotting.

Real-time polymerase chain reaction

RT-qPCR was performed in CFX96 PCR (Bio-Rad) following the manufacturer's instructions for the ChamQ SYBR qPCR Master Mix (Vazyme). We used the $2^{-\Delta\Delta CT}$ method to calculate the expressed values relative to the control. Results are represented as fold expressions. The primers sequences used for qPCR were listed as follows:

Genes	Forward (5′−3′)	Reverse (5′−3′)
β-actin	GCGAGAAGATGACCCAGATC	GGATAGCACAGCCTGGATAG
GPX4	CCTTTGCCGCCTACTGAAGC	TTCCCGAACTGGTTACACGG
HSPA5	CACGGTCTTTGACGCCAAG	CCAAATAAGCCTCAGCGGTTT
TFRC	GAGGACGCGCTAGTGTTCT	ACGCCAGACTTTGCTGAGTT
c-Myc	TCAAGAGGCGAACACACAAC	GGCCTTTTCATTGTTTTCCA

Labile iron pool (LIP) analysis

RhoNox-1 is an active fluorescent probe that combines with Fe^{2+} to form an irreversible orange fluorescent product, which has cell membrane permeability and high selectivity. Calcein acetoxymethyl ester (Cal-AM, Invitrogen, Massachusetts, USA) is a fluorescein-derived probe that can easily pass through the living cell membrane. It is metabolized in fluorescence form in the cytoplasm, and then quenched after being bound to ferrous iron (Fe^{2+}). In 6-well plates, cells (2×10^5) were treated with the indicated compounds for 72 h. After washing with PBS three times, incubated with 20 nM Cal-AM or 5 μM RhoNox-1 in Hanks Balanced Salt Solution (HBSS, Gibco, Massachusetts, USA) at 37 °C and 5% CO_2 for 30 min. Cal-AM was analyzed using a FACS Fortessa flow cytometer (BD Biosciences, California, USA), and signals were detected in the FITC channel. RhoNox-1 was analyzed via Cytation5 Cell Imaging Multi-Mode Reader (BioTek, VT, USA) using 523 nm LED in combination with an EX 531/40 EM 593/40 filter cube. For tissue, samples were digested by lysis buffer after liquid nitrogen freezing grinding. LIPs were measured by Iron concentration detection kit (BC1735, Solarbio, Beijing, China) in accordance with the manufacturer's protocol.

Glutathione determination

Intracellular reduced form glutathione (GSH) and its oxidized form GSSG were assessed using a GSH/GSSG detection assay kit (Beyotime, Shanghai, China) according to the manufacturer's instructions.

Lipid ROS analysis

Lipid ROS was stained with C11-BODIPY 581/591 (D3861, Thermo Fisher Scientific) and analyzed using flow cytometry. The cells were washed with PBS three times, incubated in HBSS (Gibco) with 5 μM C11-BODIPY 581/591 for 30 min at 37 °C and 5% CO_2 in dark. Oxidation of the polyunsaturated butadienyl portion of the dye results in a shift of the fluorescence emission peak from 590 nm to 510 nm, which could be detected on the FACS Fortessa flow cytometer (BD Biosciences) in the FITC channel.

Lentiviral-mediated shRNA transduction and TfR-1 overexpression

Parental DLBCL cell lines were transduced with lentivirus containing shRNA plasmids or overexpression plasmids at optimized viral titers. Stable cell lines were established after selection with puromycin. The pLKD-CMV-EGFP-2A-Puro-U6-shRNA (MYC) lentivirus was established by OBiO Technology Corp (Shanghai, China). shTFRC, shEED, shEZH1, and shEZH2 sequences were cloned into pLKO.1 vector individually; TFRC sequences were cloned into the

pLenti-CMV-MCS-SV-puro vector. And lentivirus was produced by HEK293T cells. The sequences used were listed as follows:

Genes	Sequences (5′–3′)
shEED	CCAGTGAATCTAATGTGACTA
shEZH1	GCTCTTCTTTGATTACAGGTA
shEZH2	CCCAACATAGATGGACCAAAT
shTFRC	CGTTGAATTGAACCTGGACTA
shNC	ACGTGACACGTTCGGAGAATT

CRISPR–Cas9-mediated knockout GPX4 in DLBCL cells
Knockout of GPX4 in human DLBCL cell lines was performed using single guide RNAs (sgRNAs). The sgRNAs were cloned into the lentiCRISPR V2 vector via homologous recombination using ClonExpress II One Step Cloning Kit (Vazyme, Nanjing, China). lentiCRISPR-sgGPX4 was co-transfected into HEK293T cells with packaging plasmid psPAX2 (12260, Addgene, Massachusetts, USA) and expressing plasmid pMD2.G (12259, Addgene). The sgRNAs for GPX4: 5′-CACGCCCGATACGCTGAGTG-3′.

Drug matrix design and cell viability assay
DLBCL cells (1×10^5) per well were seeded in 96-well plates and set in exposure or no exposure groups for 72 h at different doses of HH2853. They were, then, combined with different doses of erastin, as indicated in the Figures. After treatment, cells were incubated with 100 µL of 10% CCK-8 (Life-iLab) at 37 °C for 2 h and cell viability was assessed through absorbance at 450 nm (optical density, *OD*). The percentage inhibition was calculated from the cell viability upon treatments and used to quantify the synergy score using SynergyFinder (https://synergyfinder.fimm.fi/).

ChIP-qPCR
SimpleChIP Plus Enzymatic Chromatin IP Kit purchased from Cell Signaling Technology (#9005, CST, Massachusetts, USA), U-2932, WILL-2, KARPAS-422, and Pfeiffer cells plated in 10 cm dishes were treated with DMSO, EPZ-6438 or HH2853 for 6 days. The cells were immobilized with 1% formaldehyde for 10 min at room temperature. Glycine was then added to a final concentration of 0.125 M for 5 min. SimpleChIP® Plus Enzymatic Chromatin IP Kit (#9005, CST) was used for the ChIP-qPCR assay. Samples were processed in accordance with the manufacturer's protocol, and the following antibodies were used: anti-c-Myc (#18583, CST), anti-Histone H3K27me3 (#9733, CST), and anti-Histone H3K27ac (#39685, Active Motif). The qPCR primers targeted the gene promoter region. The primer sequences were listed as follows:

Genes	Forward (5′–3′)	Reverse (5′–3′)
MYC-promotor	AACATGACCAGACTGCCTC	CTCAAAGCAAACCTCCTAC
TFRC-promotor P1	GGCCAACATGGAGAAACC	CTCAATGCAACCTCCACC
TFRC-promotor P2	TGAGGTCAGGAATTCGA-GACAAG	GAGGAGTGACGGGATTT-TATC
TFRC-promotor P3	GGGAAGAGTAAAAGCC-CAAGG	GAACAGCCCTTTAAGAAG-CAAATC

RNA-seq and ChIP-seq analysis
We utilized RNA-seq (GEO: GSE119088) and ChIP-seq (GEO: GSE119086) data from our recent research. Gene set enrichment analysis (GSEA) was performed based on oncogenic signatures collections c6 MSigDB gene set. ChIP-seq data were analyzed by GO enrichment analysis. Raw data of RNA-seq were normalized to three replicates for GSEA analysis. The heatmap plot was by R package "ggplots".

Immunohistochemistry
We employed the multiplicative quick score method (QS) [17] to evaluate the expression of proteins. The following antibodies were used: Acetyl-Histone H3-K27 1:800 (A7253, Abclonal), H3K27me3 1:1000 (#9733, CST), TfR-1 1:100 (A5865, Abclonal), GPX4 1:100 (A1933, Abclonal) and HSPA5 1:100 (#3177, CST).

Xenograft tumor model
All animal experiments were approved by the Institutional Animal Care and Use Committee of Shanghai Institute of Materia Medica (No. 2018-05-DJ-36, No. 2021-04-DJ-62) and performed in accordance with the Association for Assessment and Accreditation of Laboratory Animal Care. Tumors were measured twice weekly and volumes were calculated using the formula $TV = \text{length} \times \text{width}^2 \times 1/2$. Individual relative tumor volume (RTV) was calculated as (TV on measured day)/ (TV at initial treatment). The T/C rate was calculated as (final RTV treatment / final RTV vehicle) × 100%.

Statistical analysis
Data were expressed as the mean ± SD from three independent experiments in all in vitro assays. Differences between groups were estimated using Student's *t* test. All these analyses were performed using GraphPad Prism 7.0 software and a two-tailed value of $P < 0.05$ was considered statistically significant.

RESULTS

Novel potent EZH1/2 inhibitor HH2853 increases H3K27 acetylation in insensitive DLBCL cells
Using a combinatorial lead-optimization strategy, we designed and synthesized HH2853 (Fig. 1a), which was systematically identified as a novel, orally bioavailable small molecule inhibitor specifically targeting EZH1 and EZH2. The in vitro methyltransferases assay showed that this compound effectively inhibited the catalytic activity of wild-type EZH2 and mutated forms (A677G, Y641F, Y641N, and Y641C) with IC_{50} of 3.75, 2.21, 2.65, and 2.62 nM, respectively, which was comparable to EPZ-6438. Notably, HH2853 synchronously suppressed EZH1 activity ($IC_{50} = 9.26 \pm 0.56$ nM), which may blunt the compensatory pathway after EZH2 inhibition (Fig. 1b). The activity of HH2853 against human lymphoma was evaluated using a panel of 24 cell lines expressing EZH2 mutations or wild type (Fig. 1c). After 10 days of treatment, the IC_{50} results showed that HH2853 had the same or a slightly stronger inhibitory effect on cancer cells proliferation than EPZ-6438. More importantly, in preclinical studies, the inhibitory ability of HH2853 at 20 mg/kg against Pfeiffer xenografts growth was much better than that of EPZ-6438 at 50 mg/kg, suggesting that HH2853 has good developmental prospects (Fig. 1d). And this compound was tolerated well, with no body weight loss in all treated groups, even HH2853 100 mg/kg group (Fig. 1d, Supplementary Fig. S1a). However, HH2853 did not show potent inhibitory effect against some lymphoma cells, the IC_{50}s of 13/24 lymphoma cell lines including 4 EZH2-WT DLBCL were >1 µM or even 10 µM. And HH2853 also did not inhibit U-2932 xenografts growth even at 100 mg/kg (Supplementary Fig. S1a). Considering that EZH2 inhibitors are undergoing clinical trials against DLBCL, we attempt to explore the resistance mechanisms of these inhibitors against DLBCL. It has been well indicated by our lab that a feedback reciprocal H3K27 acetylation (H3K27ac) upregulation may contribute to the resistance to EZH2 inhibition in cancer cells, including those with mutation [18]. Consistent with this data, H3K27ac was also upregulated in HH2853 and EPZ-6438 insensitive DLBLC cells, although H3K27 methylation was completely inhibited. Meanwhile, in EZH2i-sensitive cells, EPZ-6438

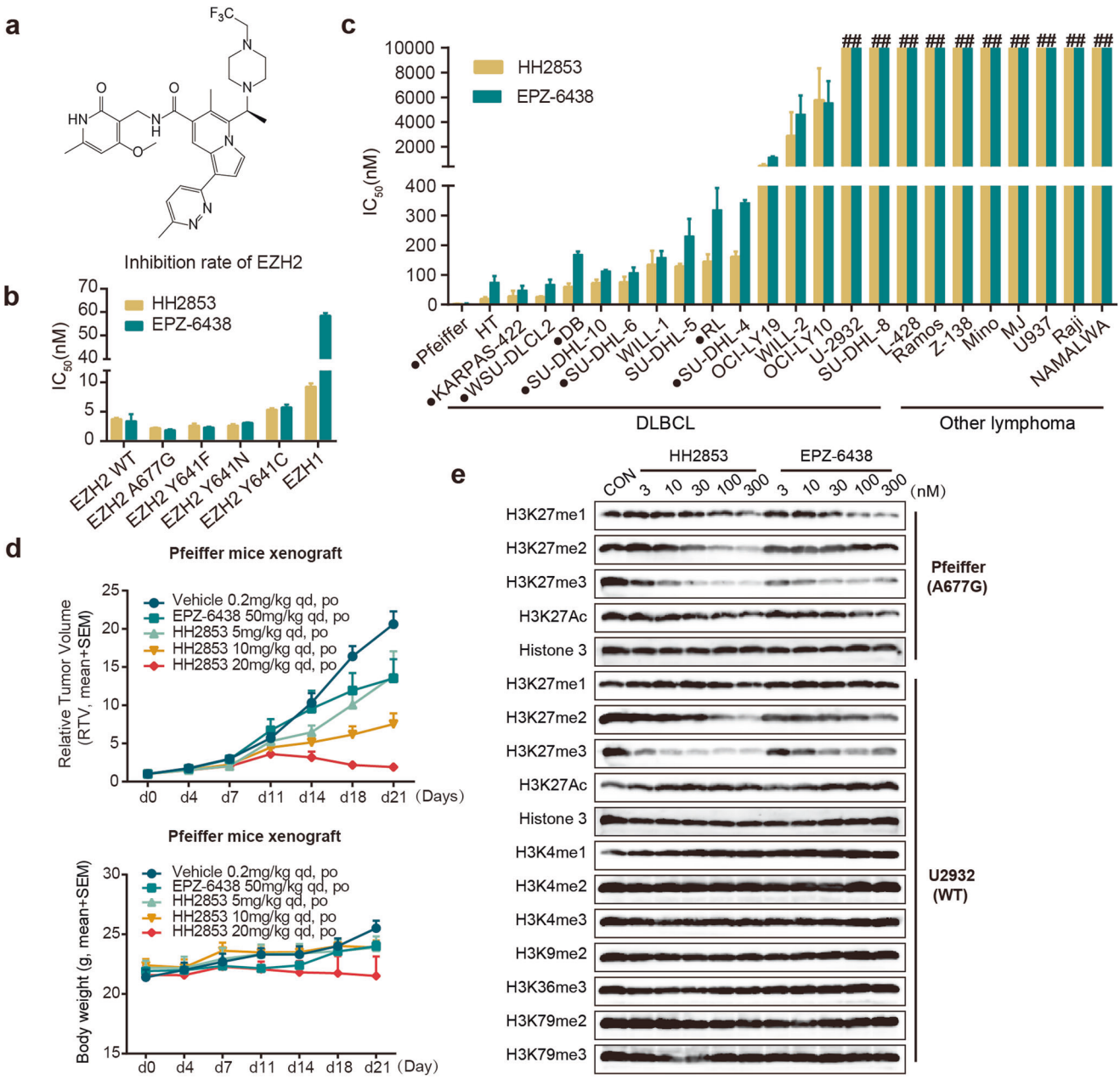

Fig. 1 HH2853 displays different responses in DLBCL in vitro and in vivo. a The structure of EZH1/2 dual inhibitor HH2853. **b** Inhibition activity of HH2853 and EPZ-6438 against EZH1 and EZH2. **c** Effects of HH2853 and EPZ-6438 on cell proliferation were tested in 24 lymphoma cell lines. IC_{50}s were measured using the CCK-8 assay after being treated with indicated inhibitors for 7 days at gradient concentrations (● means EZH2 mutant; # means $> 1 \times 10^5$ nM). **d** Anti-tumor efficacy in vivo. Mice carrying xenografts were treated with HH2853 or EPZ-6438 daily via oral gavage for the indicated days. **e** The effects of HH2853 and EPZ-6438 on histone modification in DLBCL cells were detected by immunoblotting.

and HH2853 reduced H3K27me3 and H3K27ac (Fig. 1e). Then, we attempted to explore how upregulated H3K27ac mediates EZH2i resistance in DLBCL.

EZH2 inhibition renders resistance by affecting intracellular LIP content through upregulating TfR-1

Consider that the changes in histone acetylation can affect gene transcription, RNA sequencing (RNA-seq) and chromatin immunoprecipitation sequencing (ChIP-seq) was firstly applied to find the clue. According to our in vitro and in vivo data, Pfeiffer, with lower IC_{50} and decreased H3K27ac upon EZH2i treatment, was chosen as the typical sensitive DLBCL cell to EZH2 inhibitors. Meanwhile, U-2932 was selected as a representative of insensitive cell due to the elevated H3K27ac and the IC_{50} above 10 μM after EZH2 treatment for omics studies. By integrating the RNA-seq and H3K27acChIP-seq data of U-2932 and Pfeiffer which were treated with or without EPZ-6438, the Venn diagram showed that some altered oncogenic pathways overlapped after treatment (Fig. 2a). In the analysis of two types of GO enrichment data, the top 50 pathways, besides growth, immunity, metabolism, protein synthesis, catabolism, and kinase pathway, we were excited to find that they simultaneously enriched the changes of metal ion transport pathway in EZH2i insensitive U-2932 (Fig. 2b) but not in EZH2i sensitive Pfeiffer (Supplementary Fig. S1b). Recently, cellular iron homeostasis, which has been fully proved not only essential for biological processes in normal cells, but also contributes to the growth of tumors and drug resistance by our data [10] and

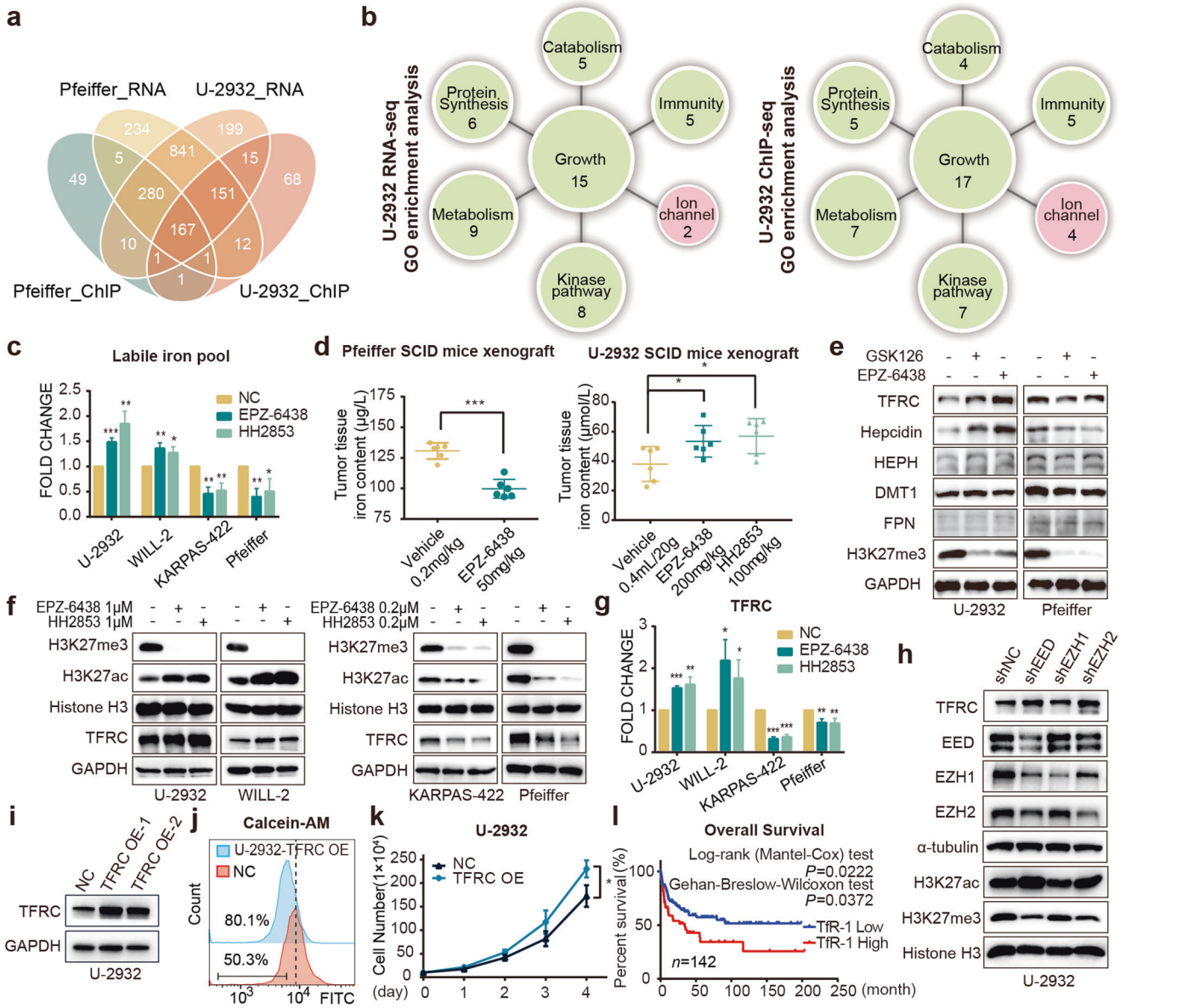

Fig. 2 EZH2 inhibition affects intracellular LIP content through TfR-1. **a** Venn diagram showing the overlap of the statistically (*P* adjust < 0.05) enriched pathways among the insensitive cell line U-2932 and sensitive cell line Pfeiffer ground on RNA-seq and ChIP-seq data. **b** GO enrichment analyzing the H3K27ac ChIP-seq and RNA-seq data influenced by EPZ-6438. Top 50 enriched pathways in U-2932 treated with EPZ-6438 compared to DMSO, divided into growth, immunity, metabolism, protein synthesis, catabolism, and kinase pathway. **c** Labile iron pool content determination assay. EPZ-6438 or HH2853 treated insensitive cell lines U-2932 and WILL-2 at 1 μM, and sensitive cell lines Pfeiffer and KASPAS-422 at 0.2 μM. Labile iron pool content was determined by FeRhoNox-1. **d** Mice carrying U-2932 or Pfeiffer xenografts were treated with EPZ-6438 or HH2853, tissue LIPs were measured. **e** Insensitive cell U-2932 was treated with 1 μM EPZ-6438 or 1 μM GSK126, and sensitive cell Pfeiffer was treated with 0.2 μM EPZ-6438 or 0.2 μM GSK126. Indicated proteins were detected. Then, insensitive cell lines U-2932 and WILL-2 were treated with 1 μM EPZ-6438 or 1 μM HH2853, and sensitive cell lines Pfeiffer and KARPAS-422 were treated with 0.2 μM EPZ-6438 or 0.2 μM HH2853. TfR-1 was detected using immunoblotting (**f**) and RT-qPCR (**g**). **h** TfR-1, H3K27me3, and H3K27ac levels were determined in U-2932 cell transfected with shEED, shEZH1, or shEZH2. **i** U-2932 cells were transfected with a lentivirus containing TfR-1-OE plasmids. The LIP (**j**) and proliferation (**k**) of U-2932-TfR-1-OE cells were examined. **l** Primary data from GSE4475 were analyzed via PrognoScan [53], and the Kaplan–Meier curve was plotted by GraphPad Prism. The statistical analysis using Student's *t* test with three biologic replicates, **P* value < 0.05; ***P* value < 0.01, ****P* value < 0.001.

literatures [9, 11], has received increasing attention. Thus, we investigated whether the changes of labile iron pool (LIP) was different between sensitive and insensitive cells after EZH2i treatment by the iron probe RhoNox-1 and Calcein-AM (Calcein-acetoxymethyl) assay. Compared with control cells, after treatment with EPZ-6438 and HH2853, cellular LIP concentration was significantly mount up in EZH2i-insensitive cells U-2932 and WILL-2, but decreased in sensitive cells Pfeiffer and KARPAS-422 (Fig. 2c). The Calcein-AM assay showed similar results. Calcein fluorescence is quenched following chelation of low-mass labile iron, thus the degree of quenching shows the amounts of chelatable iron. As shown in Fig. S1c, the MFI of Calcein fluorescence in EZH2i-treated U-2932, WILL-2, and OCI-LY10 cells were much lower than untreated cells, indicating LIP was upregulated in three EZH2i-resistant cells including U-2932, WILL-2, and OCI-LY10 cells (Supplementary Fig. S1c). Consistent with the in vitro data, a marked diminished non-heme iron content was also found in EPZ-6438 treated Pfeiffer tumor tissues, which was associated with potent tumor growth delay. In contrast, EPZ-6438 and HH2853 raised LIP in

U-2932 xenografts, and had no inhibitory effects on tumor growth (Fig. 2d, Supplementary Fig. S1a). These data suggested that an ascent in cellular iron content by EZH2 inhibition may elicit resistance. Important regulators of iron metabolism, including transferrin receptor 1 (TfR-1), hepcidin, hephaestin, DMT1, and FPN [19] were all detected after EZH2i treatment. TfR-1, the protein involved in the uptake of iron in both normal and cancer cells, was upregulated in resistant cells but downregulated in sensitive cells by EPZ-6438 HH2853, and GSK126, accompanied by attenuated H3K27me3 (Fig. 2e, f, Supplementary Fig. S1e). Synchronously, we found that the change in hepcidin was consistent with TfR-1 (encoded by *TFRC*) in cells treated with EZH2i. Hepcidin, known as the iron-regulatory hormone, usually binds to ferroportin (FPN), causing its break down, then prevents the processes of iron absorption [20, 21]. However, in our case, FPN remained unchanged in both sensitive and insensitive DLBCL cells. The data suggested that the increase of hepcidin might be due to iron overload caused by upregulated TfR-1. According to the important role of TfR-1 in the development of DLBCL [22], we first focused on TfR-1 in this study. The change in TfR-1 mRNA expression was consistent with its protein variation (Fig. 2g). Increased TfR-1, accompanied by upregulated H3K27ac and decreased H3K27me3, was also observed in EED silencing U-2932 cells (Fig. 2h). Interfering with EZH1 only slightly reduced H3K27me3 levels might be due to its low expression in DLBCL, and had almost no effect on H3K27ac and TfR-1 (Fig. 2h). To further validate the relationship between TfR-1, cell proliferation, and intracellular LIP content, we established TfR-1-overexpressing U-2932 cell line (Fig. 2i). Consistent with published data [20], when compared with parental U-2932 cells, TfR-1 overexpressing cells had a higher LIP content (Fig. 2j) and a faster proliferation rate (Fig. 2k). Furthermore, our preclinical results were also confirmed by analyzing the primary data from GSE4475 via PrognoScan [21], that high TfR-1 levels are significantly correlated with poor survival (Fig. 2l). Overall, these data suggest that EZH2 inhibition drives the upregulation of TfR-1, prompting an increase of cellular LIP, which might contribute to the resistance to EZH2i in DLBCL.

EZH2 inhibition stimulates the expression of TfR-1 by regulating c-Myc

Previous work has demonstrated that EZH2i-resistant cells exhibit feedback H3K27ac upregulation, which generally promotes oncogene expression. We hypothesized that the increased TfR-1 was caused by the upregulation of H3K27ac. To test this hypothesis, we investigated H3K27me3 and H3K27ac recruitment to the *TFRC* promoter region. EZH2i reduced H3K27me3 in both types of cell lines, but raised H3K27ac only in the resistant cell line, U-2932. In addition, in the sensitive cell line Pfeiffer, the level of H3K27ac on the promotor of *TFRC* was not altered after treatment with EZH2i (Fig. 3a and supplementary Fig. S2a).

To further understand the underlying mechanism between EZH2 and TfR-1, we analyzed the RNA-seq dataset via a Venn diagram. And 1226 signature changes were enriched (Fig. 3b). Given the role of upregulated H3K27ac in transcriptional activation, we further used gene set enrichment analysis (GSEA) to identify the genes dramatically increased in EPZ-6438-treated U-2932 while decreased in EPZ-6438 treated-Pfeiffer with $P.\text{adj} < 0.05$. A representative oncogenic signature, upregulated *MYC*, was conspicuously enriched in U-2932 cells and declined in Pfeiffer cells after treatment with EPZ-6438 (Fig. 3b). Same results were also observed in the oncogenic signature enrichment plots (Fig. 3c). This result was substantiated by detecting c-Myc mRNA and protein levels in DLBCL cells treated with EZH2i. As with the profiling data, c-Myc was noticeably increased in the insensitive U-2932 and WILL-2 cells after treatment with EPZ-6438 or HH2853 for 3 days, and was decreased in the sensitive cells, consistent with the change of TfR-1 (Fig. 3d, e). It is well known that *MYC* is a transcription factor with broad biological effects through multiple mechanisms, including target gene transcription promotion [23, 24]. As expected, c-Myc silencing reduced TfR-1 expression in 4 tested DLBCL cells (Fig. 3f). More importantly, we observed that loss of c-Myc profoundly impaired HH2853 increased-TfR-1 in U-2932 (Fig. 3g). We also detected the level of H3K27me3 and H3K27ac in the *MYC* promoter region after treatment with EZH2i for 3 days. Consistent with the ChIP-seq result (Supplementary Fig. S2a), EPZ-6438 and HH2853 inhibited the recruitment of H3K27me3 in the *MYC* promotor region in all tested DLBCL cells, and only remarkably increased H3K27ac in the *MYC* promotor region in resistant cells (Fig. 3h and supplementary Fig. S2b). Furthermore, ChIP-qPCR analysis also illustrated that in insensitive cells, increased c-Myc was recruited to the promoter of *TFRC*, which evoke the activation of TfR-1 transcription according to published data (Fig. 3i). All these indicated that EZH2i upregulates c-Myc by recruiting H3K27ac to *MYC* promoter, leading to TfR-1 enhancement in EZH2i insensitive DLBCL cells.

EZH2 inhibition stabilizes GPX4 through HSPA5 and inhibits cell ferroptosis

Ferroptosis is a cell death process caused by iron overload that mainly manifests as cellular LIP upregulation and spur cell membrane lipid peroxide accumulation, ultimately inducing cell death [25, 26]. Although it has been reported that the increase of TfR-1 can promote the growth of lymphoma, we also found inconsistent results illustrating TfR-1 as a crucial accelerator of ferroptosis [27, 28]. Based on these published data, we used C11-BODIPY, a lipid peroxidation sensor, to measure ferroptosis using flow cytometry at first. And we found that increased TfR-1 in EZH2i-resistant cells did not seem to promote the susceptibility of cells to ferroptotic cell death (Fig. 4a). Since glutathione peroxidase 4 (GPX4) is a classical and well-known ferroptosis suppressor [26, 29, 30], we first detected the effect of EZH2i on this protein and the other two ferroptosis associated proteins, FSP1 [31] and DHODH [32, 33]. And accompanied by elevated TfR-1 and c-Myc after treatment with EZH2i, notably increased GPX4 was found in the EZH2i-resistant DCBCL cells, U-2932, WILL-2 and OCI-LY10, but DHODH and FSP1 did not change (Fig. 4b). Cellular GSH, the substrate of GPX4, was also upregulated by EZH2i in resistant cells, consistent with the change in GPX4 (Fig. 4c). However, EZH2i had no obvious effect on GPX4 mRNA (Fig. 4d, g), indicating that the upregulation of GPX4 expression might be due to the change in protein stability. Cycloheximide (CHX) was used for de novo protein synthesis inhibition. As expected, in the cells treated with CHX alone, GPX4 was reduced, and EZH2i together with CHX still elevated the protein level of GPX4 (Fig. 4e). In addition, we found that treatment with EPZ-6438 and HH2853 did not markedly increase GPX4 ubiquitination in U-2932 cells (Fig. 4f). A recent study showed that heat shock protein family A (Hsp70) member 5 (HSPA5) bind to GPX4 and slow down its degradation [34]. RNA-seq data revealed that HSPA5 was apparently increased by EZH2i only in the insensitive cell U-2932, which was confirmed by qPCR analysis (Fig. 4g, h). This result was substantiated by detecting the protein levels of HSPA5 in EZH2i-treated U-2932, WILL-2, and OCI-LY10. Similar to the change in GPX4, EZH2i combined with CHX also reversed CHX-induced downregulation of HSPA5 in EZH2i insensitive cells (Fig. 4e). Co-IP assay displayed that EZH2i promoted the binding of HSPA5 to GPX4 in U-2932 cells (Fig. 4i), which might improve GPX4 stability. TfR-1 overexpression increased HSPA5 mRNA and protein levels in U-2932 cells. And TfR-1 depletion suppressed HSPA5 expression in this cell line (Fig. 4j, k). Overall, these results demonstrate that EZH2i-upregulated HSPA5 stabilizes GPX4, thereby helping EZH2i-resistant DLBCL cells escape ferroptosis.

The combination of EZH2i and erastin induces ferroptosis in EZH2i-resistant DLBCL cells

As GPX4 plays a crucial role in ferroptosis, we aimed to determine whether blocking the GPX4 pathway could overcome resistance to

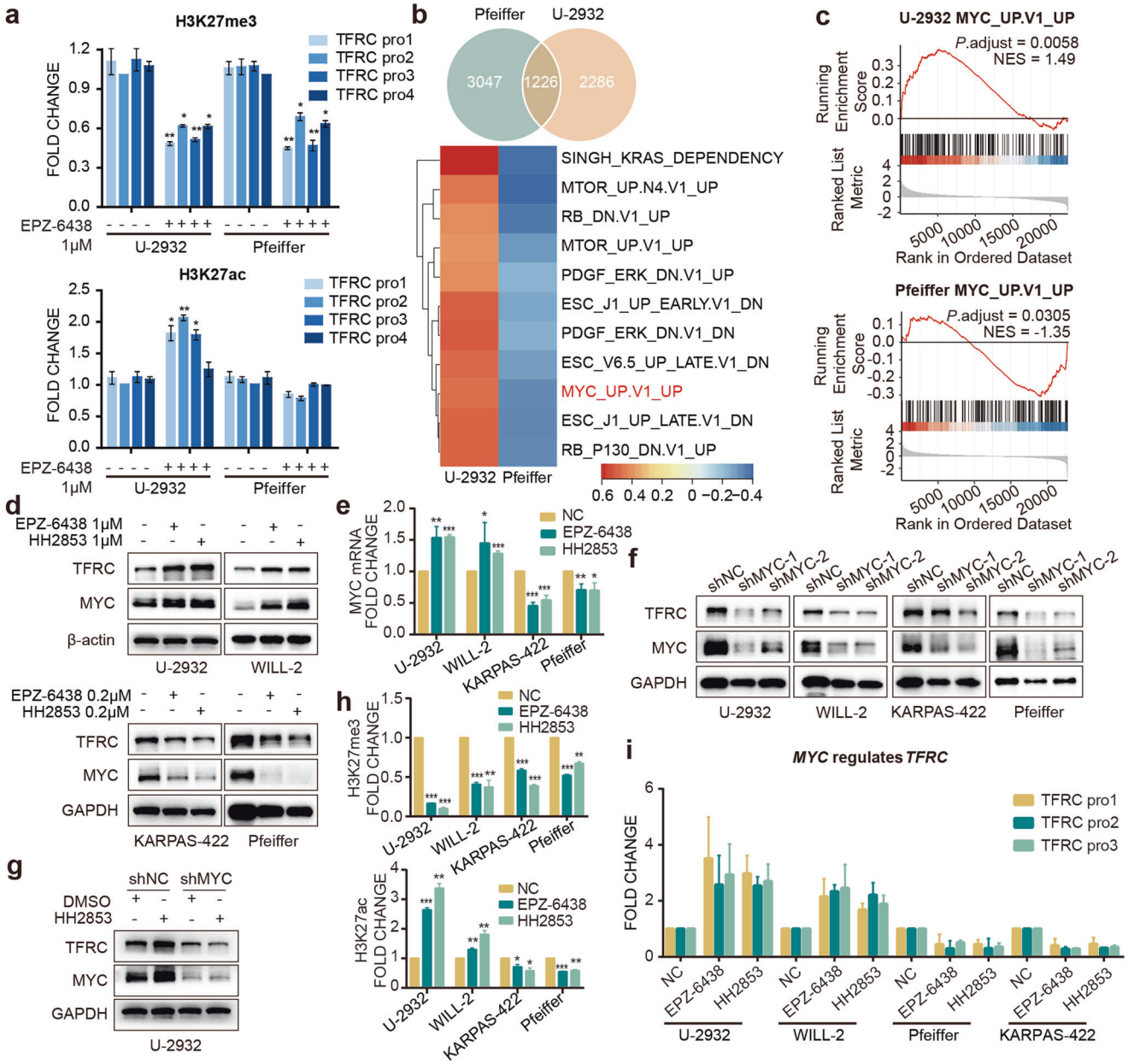

Fig. 3 EZH2i affects the expression of TfR-1 by regulating c-Myc. a ChIP-qPCR verified the histone modification changes in the TfR-1 promoter region. **b** Venn diagram showing the differential expression of the statistically (*P* adjust < 0.05) enriched genes among the insensitive cell line U-2932 and the sensitive cell line Pfeiffer. GSEA analysis (using oncogenic c6 MSigDB gene set) of H3K27ac ChIP-seq data affected by EPZ-6438. The heatmap showing the enriched pathways (*P* adjust < 0.05) in the oncogenic signatures from the Molecular Signatures Database (MSigDB) with EPZ-6438 compared to DMSO treated U-2932 and Pfeiffer. The color was based on the enrichment score. **c** Oncogenic signature enrichment plots of H3K27ac ChIP-seq with EPZ-6438 treatment compared with DMSO treatment in U-2932. Plots indicate a significant (FDR *q* < 0.05) enrichment of oncogenic signatures after EPZ-6438 treatment. **d**, **e** c-Myc mRNA and protein levels were altered in cells treated with EPZ-6438 or HH2853 for 3 days. **f** DLBCL cells were transfected with lentivirus to deplete c-Myc expression. The indicated proteins in cells treated with or without 1 μM HH2853 were analyzed by immunoblotting (**g**). The histone modification changes in the *MYC* promoter region (**h**) and the c-Myc binding changes in the *TFRC* promoter region (**i**) were verified by ChIP-qPCR. The statistical analysis using Student's *t* test with three biologic replicates, **P* value < 0.05; ***P* value < 0.01, ****P* value < 0.001.

EZH2i. We established GPX4-KO U-2932 using CRISPR–Cas9 (Fig. 5a) and measured cell viability after treatment with HH2853 (Fig. 5b). The results showed that compared with GPX4-KO U-2932, ferrostatin-1(Fer), a ferroptosis inhibitor, stimulated cells proliferation as expected. HH2853 at 1 μM almost completely inhibited proliferation of GPX4-depleted U-2932 cells in vitro. In contrast, at this dose, HH2853 did not affect parental U-2932 cells. As expected, Fer weakened the inhibitory effect of HH2853 on this cell line. The data indicate that loss of GPX4 could restore sensitivity to EZH2 inhibitors. The classical ferroptosis inducer, erastin [35], was used to investigate the sensitization effect. DLBCL cells in the combination group were pre-treated with EZH2i for 3 days and then co-treated with erastin for another 24 h. As measured by C11-BODIPY via flow cytometry, we found that EZH2i alone did not affect ferroptosis, furthermore, erastin alone and the combination therapy potently precipitate ferroptosis in EZH2i resistant DLBCL cells (Fig. 5c). Fer reversed the effect of the combination treatment. The proliferation inhibitory effect of

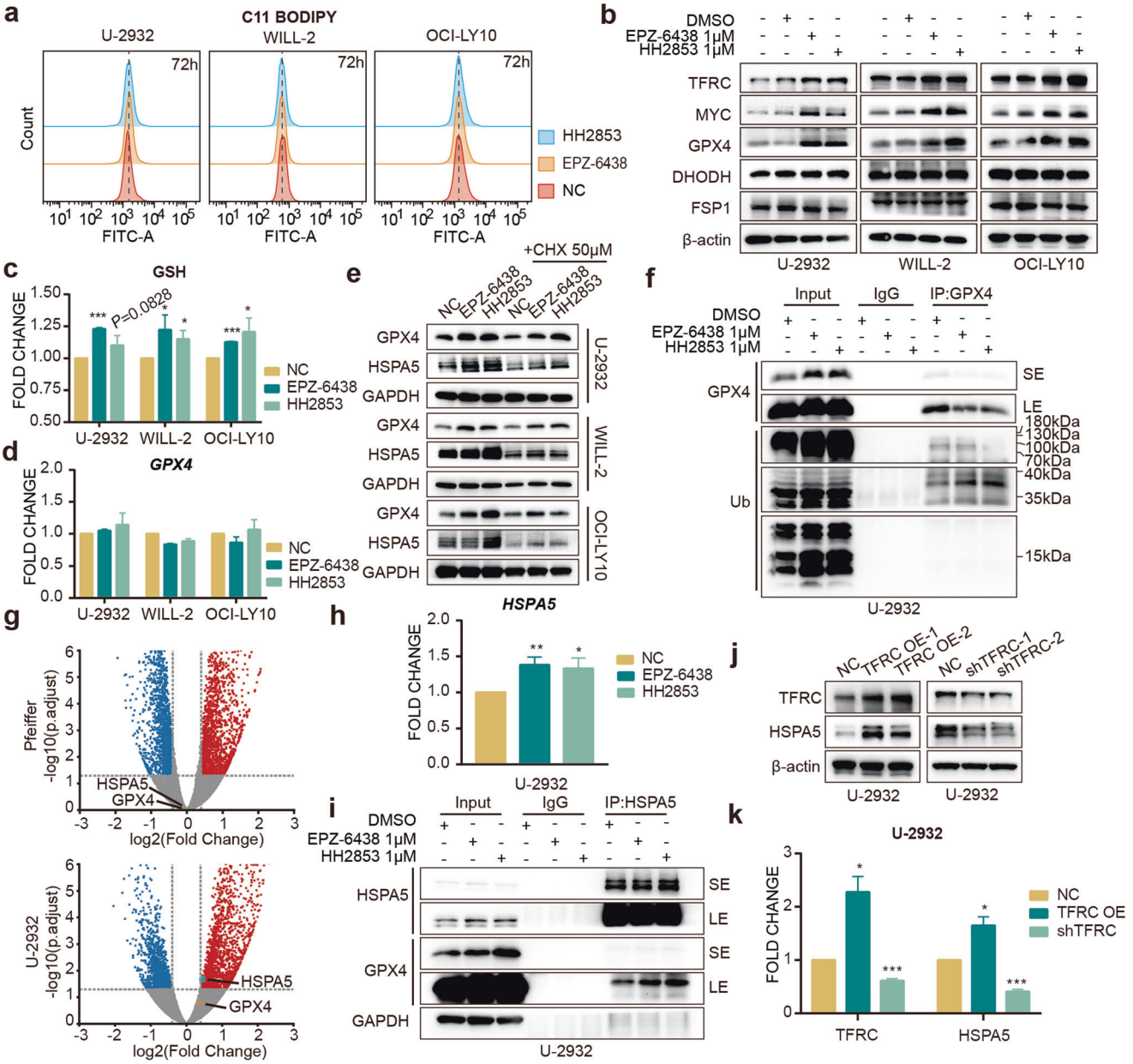

Fig. 4 EZH2i stabilizes GPX4 through HSPA5 and inhibits cell ferroptosis. a Cells were treated with 1 μM EPZ-6438 or 1 μM HH2853 for 3 days, and lipid ROS levels were determined by C11-BODIPY (**b**–**d**). Cells were treated with EZH2i for 3 days. GPX4, DHODH, and FSP1 protein levels were detected (**b**) by Western blot, glutathione was determined using the GSH/GSSG Detection Assay Kit (**c**). and GPX4 mRNA levels were measured by RT-qPCR (**d**). **e** CHX did not reverse EZH2i-induced GPX4 and HSPA5 upregulation. **f** Co-immunoprecipitation (Co-IP) indicated that EZH2i cannot facilitate the GPX4 polyubiquitylation (**g**) Volcano plot. The volcano plot illustrates the fold changes of genes after treatment with EPZ-6438 in U-2932 and Pfeiffer cells compared to DMSO-treated cells. The corresponding adjusted p-values were calculated for the three biological replicates. The upregulated genes are shown in red, downregulated genes are shown in blue, and statistically insignificant genes are shown in gray. **h** EZH2i increased HSPA5 mRNA level in EZH2i resistant U-2932 cells treated with 1 μM EPZ-6438 or 1 μM HH2853 for 3 days. **i** Co-immunoprecipitation (Co-IP) indicated that EZH2i increased GPX4 binding to HSPA5. Cell lysates were incubated with anti-GPX4 or immunoglobulin G (IgG) antibodies. Immunoblot indicated the alteration of immunoprecipitates. SE: short exposure, LE: long exposure. Protein and mRNA levels of HSPA5 were determined in TfR-1 overexpressed and depleted U-2932 cells (**j**, **k**). The statistical analysis using Student's *t* test with three biologic replicates, **P* value < 0.05; ***P* value < 0.01, ****P* value < 0.001.

HH2853 plus erastin was also assessed. After exposure to EZH2i for 3 days then co-treated with erastin for another 24 h, compared with HH2853 or erastin alone, a more significant suppressive effect was observed (Fig. 5d). When the co-treatment time with EZH2i and erastin was extended to 4 days, more gratifying results were observed in the combination group (Fig. 5e and supplementary S2c). We used the SynergyFinder algorithm for combination analysis and employed three well-established pharmacological models (HSA, Bliss, and ZIP). As shown in the table, all resistant cell proliferation was blunted by EZH2i + erastin; contemporarily, they had stronger impairment at some concentrations in the three methods. Further, GPX4 specific covalent binding inhibitors RSL3 or ML162 also have shown synergistic effects when combined with EZH2i. DLBCLs were pre-treated for 3 days with EZH2i to persist before 8 h of combination with GPX4i for FACS verification (Fig. 5f) and 72 h for the proliferation test (Fig. 5g). Together, these

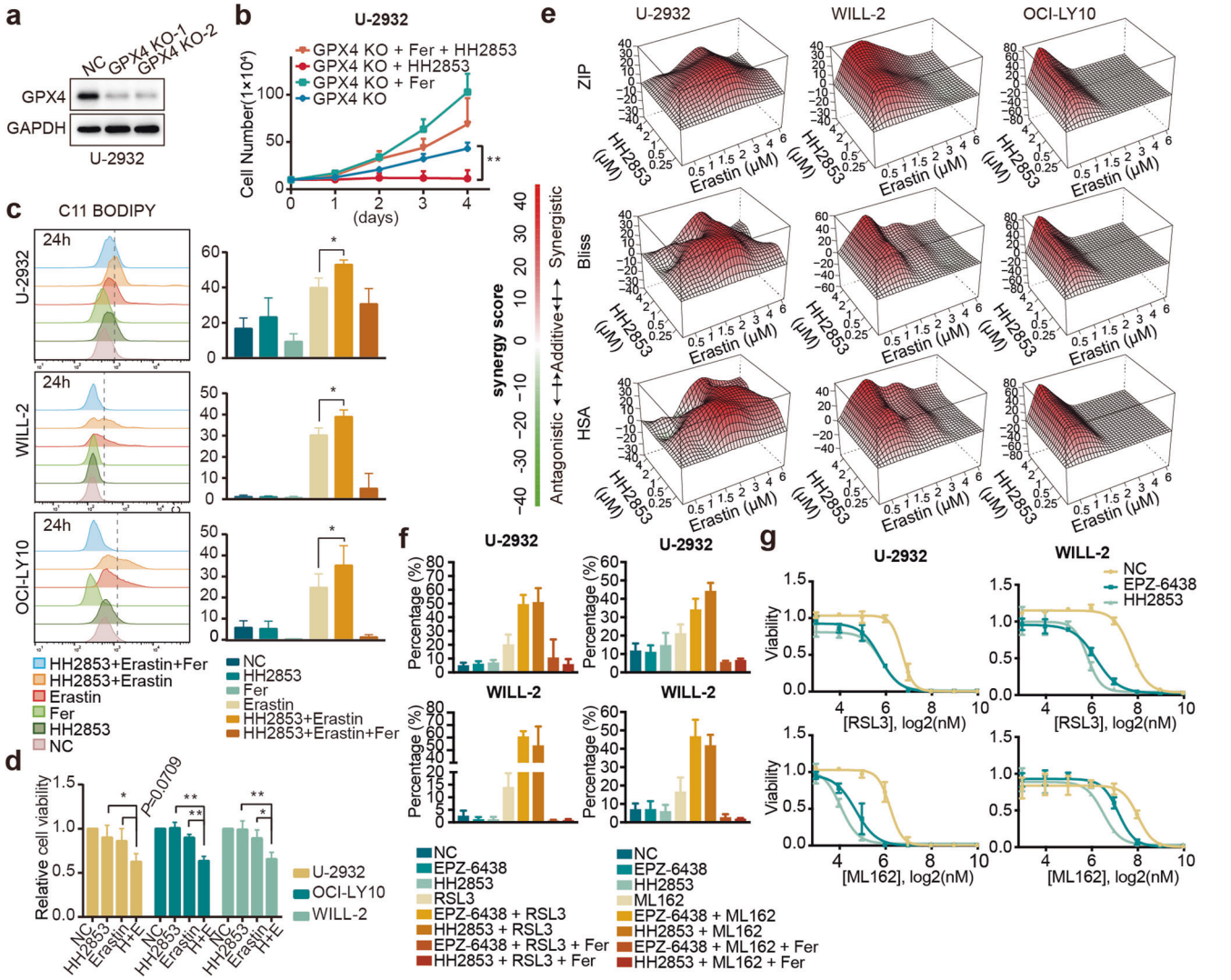

Fig. 5 Combination of EZH2i and Erastin induced ferroptosis of drug-resistant cells. a CRISPR–Cas9 mediated knockout of GPX4 in U-2932 cells. **b** The viability of GPX4-KO cells treated with 1 μM HH2853, 5 μM Ferrostatin-1 (Fer) alone, or both (5 μM Ferrostatin-1 + 1 μM HH2853) was determined using a cell counter. **c** Lipid ROS levels were determined in DLBCL cells after treatment with 1 μM HH2853, 5 μM Ferrostatin-1 (Fer), 5 μM erastin, 1 μM HH2853 + 5 μM erastin, or 1 μM HH2853 + 5 μM Ferrostatin-1 + 5 μM erastin for 24 h. Cells were exposed to HH2853 for 3 days before treatment with erastin. The histogram shows three individual experiments. **d** Cell viability was determined after treatment with 1 μM HH2853, 10 μM erastin, or 1 μM HH2853 + 10 μM erastin (E + H) for 24 h. Cells in the HH2853 group and E + H group were exposed to HH2853 for 3 days before treatment with indicate inhibitor. **e** SynergyFinder analysis of synergistic effects. Three EZH2i-resistant DLBCL cell lines were treated with a combination of HH2853 and erastin at the indicated doses for 3 days after HH2853 pretreatment for 3 days. Cell viability was measured using a CCK-8 assay. Synergy scores and 3D surface plots of cell viability in the three EZH2i-resistant DLBCL cell lines were quantified and analyzed with HSA, ZIP, and Bliss models using SynergyFinder ($n = 3$ independent experiments for each cell line). **f** Lipid ROS levels were determined in DLBCL cells after treatment with 1 μM EZH2i (EPZ-6438 or HH2853), 2 μM GPX4i (RSL3 or ML162), 1 μM EZH2i + 2 μM GPX4i, or 1 μM EZH2i + 5 μM Ferrostatin-1 + 2 μM GPX4i for 8 h. Cells were exposed to EZH2i for 3 days before treatment with GPX4i. The histogram shows three individual experiments. **g** Two EZH2i-resistant DLBCL cell lines were treated with a combination of EZH2i (EPZ-6438 or HH2853) and GPX4i (RSL3 or ML162) at the indicated doses for 3 days after 1 μM EZH2i pretreatment for 3 days. Cell viability was measured using a CCK-8 assay. The statistical analysis using Student's *t* test with three biologic replicates, **P* value < 0.05; ***P* value < 0.01.

data indicate that ferroptosis inducers promote the anti-proliferative potency of EZH2i against EZH2i insensitive DLBCL cell lines.

Erastin synergistically inhibits DLBCL xenografts growth with EZH2i

Further, we evaluated whether erastin could overcome the resistance to EZH2i in vivo. In the WILL-2 xenograft model, HH2853 and erastin alone suppressed tumor growth with an inhibitory rate of 22.85% and 30.37%, respectively. Although the poor PK property of erastin weakened its antitumor effect in vivo, a combination of HH2853 and erastin still more potently inhibited tumor growth compared to each compound alone and vehicle, yielding an inhibitory rate of 53.85% (Fig. 6a and Supplementary S1d). As expected, according to Western blotting and IHC analysis, the enhanced in vivo antitumor activity of erastin plus HH2853 was also associated with the reversal of GPX4 by erastin, although HH2853 alone increased TfR-1 and GPX4 in xenografts (Fig. 6b, c). And the content of iron was still upregulated in tumor tissues treated with HH2853 (Fig. 6d). Together, these data suggest that the simultaneous targeting of GPX4 may provide a therapeutic option to overcome primary resistance in DLBCL based on epigenetic therapy.

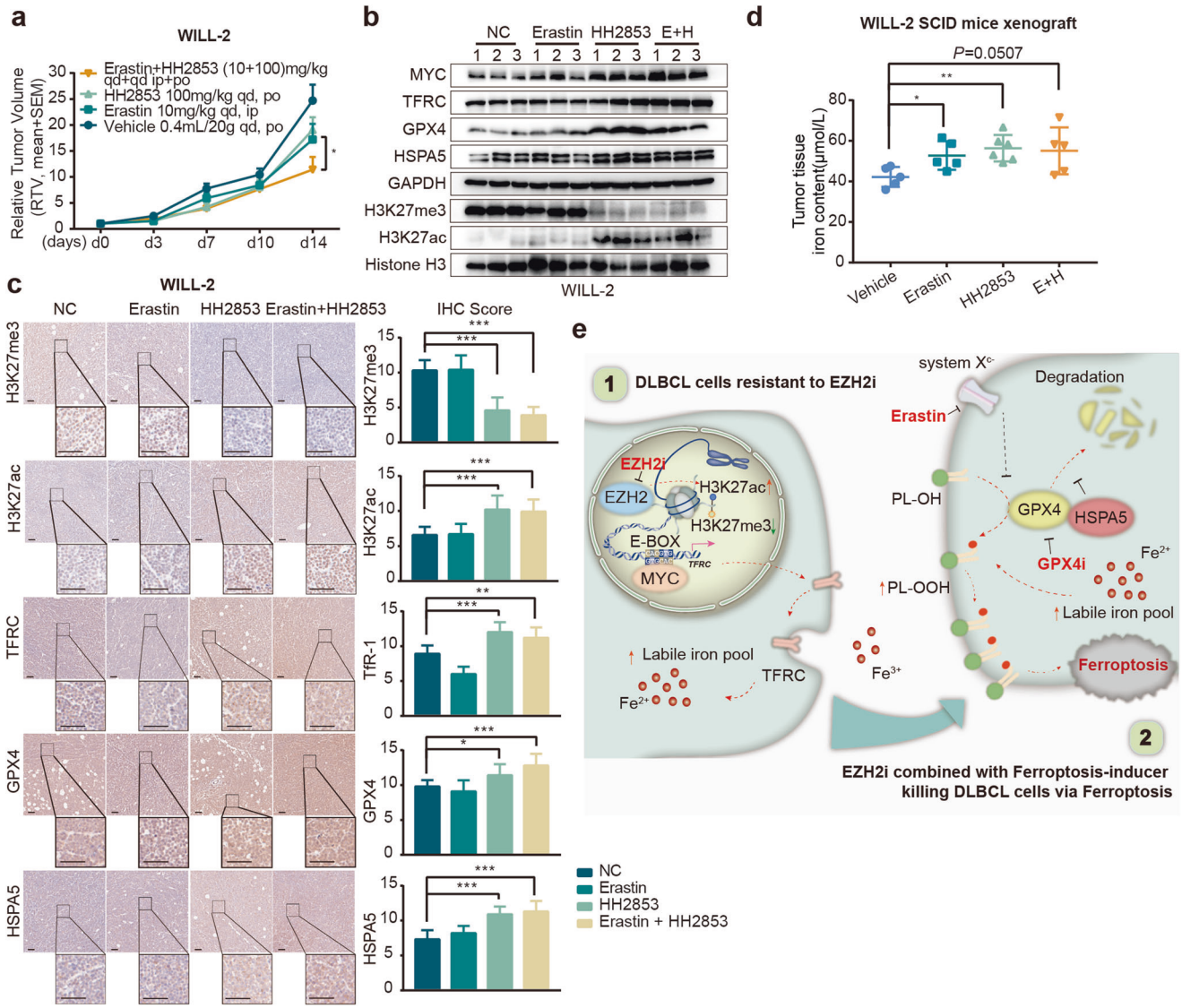

Fig. 6 EZH2i and Erastin synergistically inhibit DLBCL xenografts growth. Mice carrying WILL-2 xenografts were treated with HH2853 or erastin alone or in combination at the indicated dosages daily for the indicated days. The tumor growth curve is shown (**a**), and intratumoral levels of the indicated proteins were measured by immunoblotting (**b**) or IHC (**c**). Scale bar, 50 μm. **d** The iron content of WILL-2 xenografts was measured. **e** Schematic diagram of DLBCL resistance induced by EZH2i. The statistical analysis using Student's *t* test with three biologic replicates, **P* value < 0.05; ***P* value < 0.01, ****P* value < 0.001.

DISCUSSION

DLBCL is the most common non-Hodgkin's lymphoma worldwide, accounting for more than 18,000 newly diagnosed patients every year [36, 37]. Although chemotherapy and immunotherapy have achieved great success in the treatment of DLBCL, nearly one-third of patients develop recurrent or progressive disease, which is typically fatal [36]. Hence, an urgent need to develop novel therapeutic approaches for DLBCL cure prevails. It has been well interpreted that epigenetic regulation by PRC2 is essential in controlling DLBCL through mediating histone methylation at H3K27. A series of EZH2 inhibitors, including 3-dezaneplanocin-A (DZNep), GSK126, and especially EPZ-6438, have confirmed antitumor effects for the treatment of some DLBCL preclinical models [38, 39]. All of these aspects combine to make it a viable anti-cancer target in present epigenetic strategies [40, 41]. Here, we found that HH2853, a potent EZH1/2 dual inhibitor, exhibits a more dramatic anti-tumor effect against DLBCL, possibly owing to its favorable PK properties in preclinical studies and dual inhibition of EZH1 and EZH2. Currently, it is in phase I clinical development with high tolerability and bright development prospects.

Regrettably, as other reported dual inhibitors [42], HH2853 demonstrated considerably better antitumor effect in the sensitive DLBCL models, HH2853 and other EZH2 inhibitors alone still confront the dilemma of primary drug resistance, especially in EZH2-WT DLBCL. Therefore, it is vital to explore the molecular mechanisms underlying primary resistance. According to a review of published publications, numerous types of cancer have an elevated demand for iron, notably in DLBCL, as iron is directly associated with cell proliferation and growth. It has also been revealed dysregulation of assorted iron-related proteins, such as TfR-1 and DMT1, might alter the occurrence and progression of leukemia [43–45]. We observed that amplification of TfR-1, the major iron importer, is accompanied with inflated intracellular iron levels and encouraged DLBCL cell growth in vitro. Another striking observation is that raised TfR-1 expression is substantially related with poor survival in DLBCL patients. Additionally, several studies

have found that elevated iron levels are linked to cancer medication resistance. TfR-1 has been shown to be risen in MCF-7 cells resistant to cisplatin and doxorubicin [11]. Similarly, TfR-1 expression has been discovered to be augmented in doxorubicin-resistant human chronic myelogenous leukemia cells and promyelocytic leukemia cells [46], while dropped in gallium-resistant HL60 cells [47]. In this investigation, we demonstrated for the first time that EZH2 inhibition upregulated-TfR-1 dysregulation leads to drug resistance in EZH2 WT DLBCL. Our findings shed light on EZH2, which regulates resistance by influencing cellular iron homeostasis, and suggested that the quantity of cellular iron in tumor tissues might predict EZH2i resistance in DLBCL.

This study also highlighted the detailed mechanism of TfR-1 regulation by EZH2. Our previously published work well validated that the feedback augments of H3K27ac caused by EZH2 inhibition diminished the cell response to EZH2i [18]. For this purpose, we initially assumed that the upregulation of TfR-1 was mainly mediated by H3K27 acetylation. Despite increased H3K27ac could be recruited to *TFRC* promoter in EZH2i-treated insensitive DLBCL cells, a corresponding reduction in H3K27ac was not detected in sensitive cell lines with TfR-1 downregulation. As mentioned in earlier reports, c-Myc greatly enhances TfR-1 expression [48, 49]. We proved that EZH2 inhibitors act as a positive regulator of TfR-1 expression by recruitment of c-Myc binding to the TfR-1 promoter, which provokes iron accumulation and facilitates DLBCL cells proliferation. Collectively, these finding may partially explain the poor efficacy of EZH2 inhibition as monotherapy against DLBCL.

Based on the pivotal role of iron in EZH2 inhibition resistance, we focused on discovering iron-targeted strategies to overcome resistance in this study. Ferroptosis is a newly discovered, intracellular iron-dependent, non-apoptotic form of cell death, and is considered a promising new means to treat cancer. Previous studies have found that suppression of ferroptosis causes resistance to anti-PD-1/PD-L1 therapy, and spur ferroptosis elicits increased sensitivity to gefitinib in TNBC cells [50]. Some literatures have shown that elevated intracellular LIP and TfR-1 can trigger ferroptosis [25, 26]. However, no distinct ferroptosis occurred in insensitive DLBCL cells treated with EZH2i, while EZH2 inhibition stimulated iron and TfR-1 in these cells. This should be one of the mechanisms leading to resistance to EZH2i. As the most important pathway governing ferroptosis, we examined the GPX4-regulated pathway in EZH2i-treated DLBCL [29, 51, 52]. In this case, upregulated HSPA5 by EZH2i stabilized GPX4, thereby suppressing ferroptosis and inducing resistance to EZH2i in DLBCL. Therefore, pharmacological regulation of ferroptosis has been attempted to overcome EZH2i resistance. As expected, erastin, an inducer of ferroptosis, combined with EZH2i led to ferroptosis through perturbing GPX4 there by synergistically inhibiting EZH2i insensitive DLBCL growth in vitro and in vivo.

CONCLUSIONS

In this study, we introduced a novel EZH1/2 dual inhibitor HH2853 with more powerful antitumor activity. More importantly, we found that EZH2 restriction induced TfR-1 and LIP increase, prompted cell growth, ultimately precipitated EZH2i resistance and treatment failure in DLBCL. In insensitive DLBCL cells, aberrant EZH2 function promoted HSPA5 binding to GPX4 by upregulating HSPA5 transcription, stabilizing GPX4, eluding its degradation, which finally induced anergy of ferroptosis. It implied that predominant insensitive DLBCL cells may be unanimously vulnerable to GPX4 pathway impairment. To circumvent this issue, we are looking to drug combinations for an optimal solution. The ferroptosis inducers, exert effects by GSH deprivation or impede the activity of suppresser, combining with EZH2i reversed the upregulation of GPX4, synergistically evoked ferroptosis, and restrained EZH2i-resistant DLBCL growth in vitro and in vivo (Fig. 6e). Our study provides innovative insight into EZH2i, which elicits resistance by dysregulation of iron homeostasis in DLBCL and provides a rationale for EZH2i in combination with a ferroptosis inducer. That would appear to be a pretty compelling integrated approach for EZH2-WT DLBCL patients' cure in clinical trials.

ACKNOWLEDGEMENTS

This work was supported by grants from Program of Shanghai Academic Research Leader (22XD1404400), the Strategic Priority Research Program of the Chinese Academy of Sciences (XDA12020233), Youth Innovation Promotion Association of Chinese Academy of Sciences (2020281) and Lingang Laboratory (LG202103-02-05). We thank Haihe Biopharma Co., Ltd. for providing HH2853.

AUTHOR CONTRIBUTIONS

YC, YFF, JD, and LY designed the experiments. LY, YFW, JX, QQS, SSC, and DZL performed the research. LY and YFW analyzed the data, LY and JX wrote the paper which was revised by JD, YFF, and YC. All authors approved the final version of the paper.

ADDITIONAL INFORMATION

Supplementary information The online version contains supplementary material available at https://doi.org/10.1038/s41401-023-01097-4.

Competing interests: JD is the Chairman of Haihe Biopharma Co., Ltd. No competing interests is disclosed for rest of the authors.

REFERENCES

1. Di Croce L, Helin K. Transcriptional regulation by Polycomb group proteins. Nat Struct Mol Biol. 2013;20:1147–55.
2. Duan R, Du W, Guo W. EZH2: a novel target for cancer treatment. J Hematol Oncol. 2020;13:104.
3. Eich ML, Athar M, Ferguson JE 3rd, Varambally S. EZH2-targeted therapies in cancer: hype or a reality. Cancer Res. 2020;80:5449–58.
4. Knutson SK, Kawano S, Minoshima Y, Warholic NM, Huang KC, Xiao Y, et al. Selective Inhibition of EZH2 by EPZ-6438 leads to potent antitumor activity in *EZH2*-mutant non-Hodgkin lymphoma. Mol Cancer Ther. 2014;13:842.
5. Morschhauser F, Tilly H, Chaidos A, McKay P, Phillips T, Assouline S, et al. Tazemetostat for patients with relapsed or refractory follicular lymphoma: an open-label, single-arm, multicentre, phase 2 trial. Lancet Oncol. 2020;21:1433–42.
6. Italiano A, Soria J-C, Toulmonde M, Michot JM, Lucchesi C, Varga A, et al. Tazemetostat, an EZH2 inhibitor, in relapsed or refractory B-cell non-Hodgkin lymphoma and advanced solid tumours: a first-in-human, open-label, phase 1 study. The Lancet Oncology. 2018;19:649–59.
7. McCabe MT, Ott HM, Ganji G, Korenchuk S, Thompson C, Van Aller GS, et al. EZH2 inhibition as a therapeutic strategy for lymphoma with EZH2-activating mutations. Nature. 2012;492:108–12.
8. Torti SV, Torti FM. Iron and Cancer: 2020 Vision. Cancer Res. 2020;80:5435–48.
9. Wang Y, Yu L, Ding J, Chen Y. Iron metabolism in cancer. Int J Mol Sci. 2018;20:95.
10. Wang YF, Zhang J, Su Y, Shen YY, Jiang DX, Hou YY, et al. G9a regulates breast cancer growth by modulating iron homeostasis through the repression of ferroxidase hephaestin. Nat Commun. 2017;8:274.
11. Kazan HH, Urfali-Mamatoglu C, Gunduz U. Iron metabolism and drug resistance in cancer. Biometals. 2017;30:629–41.
12. Shen Z, Song J, Yung BC, Zhou Z, Wu A, Chen X. Emerging strategies of cancer therapy based on ferroptosis. Adv Mater. 2018;30:e1704007–e.
13. Dixon SJ, Lemberg KM, Lamprecht MR, Skouta R, Zaitsev EM, Gleason CE, et al. Ferroptosis: an iron-dependent form of nonapoptotic cell death. Cell. 2012;149:1060–72.
14. Hangauer MJ, Viswanathan VS, Ryan MJ, Bole D, Eaton JK, Matov A, et al. Drug-tolerant persister cancer cells are vulnerable to GPX4 inhibition. Nature. 2017;551:247–50.
15. Hassannia B, Vandenabeele P, Vanden Berghe T. Targeting ferroptosis to iron out cancer. Cancer Cell. 2019;35:830–49.
16. Chen XX, Shen QQ, Zhao Z, Fang YF, Yang JY, Gao YL, et al. Abstract 5436: HH2853 is a selective small molecular dual inhibitor of EZH1/2 with potent anti-tumor activities. Cancer Res. 2022;82:5436.

17. Huang X, Yan J, Zhang M, Wang Y, Chen Y, Fu X, et al. Targeting epigenetic crosstalk as a therapeutic strategy for EZH2-aberrant solid tumors. Cell. 2018;175:186–99.e19.
18. Liu Y, Gu Y, Han Y, Zhang Q, Jiang Z, Zhang X, et al. Tumor Exosomal RNAs Promote Lung Pre-metastatic Niche Formation by Activating Alveolar Epithelial TLR3 to Recruit Neutrophils. Cancer Cell. 2016;30:243–56.
19. Morales M, Xue X. Targeting iron metabolism in cancer therapy. Theranostics. 2021;11:8412–29.
20. Nemeth E, Ganz T. Hepcidin and iron in health and disease. Annu Rev Med. 2023;74:261–77.
21. Ganz T, Nemeth E. Hepcidin and iron homeostasis. Biochim Biophys Acta. 2012;1823:1434–43.
22. Lu B, Chen XB, Ying MD, He QJ, Cao J, Yang B. The role of ferroptosis in cancer development and treatment response. Front Pharmacol. 2018;8:992.
23. Yang H, Said AM, Huang H, Papa APD, Jin G, Wu S, et al. Chlorogenic acid depresses cellular bioenergetics to suppress pancreatic carcinoma through modulating c-Myc-TFR1 axis. Phytother Res. 2021;35:2200–10.
24. O'Donnell KA, Yu D, Zeller KI, Kim JW, Racke F, Thomas-Tikhonenko A, et al. Activation of transferrin receptor 1 by c-Myc enhances cellular proliferation and tumorigenesis. Mol Cell Biol. 2006;26:2373–86.
25. Lu Y, Yang Q, Su Y, Ji Y, Li G, Yang X, et al. MYCN mediates TFRC-dependent ferroptosis and reveals vulnerabilities in neuroblastoma. Cell Death Dis. 2021;12:511.
26. Wu J, Minikes AM, Gao M, Bian H, Li Y, Stockwell BR, et al. Intercellular interaction dictates cancer cell ferroptosis via NF2-YAP signalling. Nature. 2019;572:402–6.
27. Ooko E, Saeed ME, Kadioglu O, Sarvi S, Colak M, Elmasaoudi K, et al. Artemisinin derivatives induce iron-dependent cell death (ferroptosis) in tumor cells. Phytomedicine. 2015;22:1045–54.
28. Tang LJ, Zhou YJ, Xiong XM, Li NS, Zhang JJ, Luo XJ, et al. Ubiquitin-specific protease 7 promotes ferroptosis via activation of the p53/TfR1 pathway in the rat hearts after ischemia/reperfusion. Free Radic Biol Med. 2021;162:339–52.
29. Yang WS, SriRamaratnam R, Welsch ME, Shimada K, Skouta R, Viswanathan VS, et al. Regulation of ferroptotic cancer cell death by GPX4. Cell. 2014;156:317–31.
30. Bebber CM, Thomas ES, Stroh J, Chen Z, Androulidaki A, Schmitt A, et al. Ferroptosis response segregates small cell lung cancer (SCLC) neuroendocrine subtypes. Nat Commun. 2021;12:2048.
31. Bersuker K, Hendricks JM, Li Z, Magtanong L, Ford B, Tang PH, et al. The CoQ oxidoreductase FSP1 acts parallel to GPX4 to inhibit ferroptosis. Nature. 2019;575:688–92.
32. Mao C, Liu X, Zhang Y, Lei G, Yan Y, Lee H, et al. DHODH-mediated ferroptosis defence is a targetable vulnerability in cancer. Nature. 2021;593:586–90.
33. Wang F, Min J. DHODH tangoing with GPX4 on the ferroptotic stage. Signal Transduct Target Ther. 2021;6:244.
34. Zhu S, Zhang Q, Sun X, Zeh HJ 3rd, Lotze MT, Kang R, et al. HSPA5 regulates ferroptotic cell death in cancer cells. Cancer Res. 2017;77:2064–77.
35. Zhao Y, Li Y, Zhang R, Wang F, Wang T, Jiao Y. The role of erastin in ferroptosis and its prospects in cancer therapy. Onco Targets Ther. 2020;13:5429–41.
36. Lu Y, Zhao YL, Xiong M, Sun RJ, Cao XY, Wei ZJ, et al. Unmanipulated haploidentical donor and matched unrelated donor hematopoietic stem cell transplantation in patients with paroxysmal nocturnal hemoglobinuria: a single-center study. Leuk Lymphoma. 2022;63:1211–9.
37. Devin J, Cañeque T, Lin YL, Mondoulet L, Veyrune JL, Abouladze M, et al. Targeting cellular iron homeostasis with ironomycin in diffuse large B-cell lymphoma. Cancer Res. 2022;82:998–1012.
38. Genta S, Pirosa MC, Stathis A. BET and EZH2 inhibitors: novel approaches for targeting cancer. Curr Oncol Rep. 2019;21:13.
39. Tremblay-LeMay R, Rastgoo N, Pourabdollah M, Chang H. EZH2 as a therapeutic target for multiple myeloma and other haematological malignancies. Biomark Res. 2018;6:34.
40. Deb G, Singh AK, Gupta S. EZH2: not EZHY (easy) to deal. Mol Cancer Res. 2014;12:639–53.
41. Sermer D, Pasqualucci L, Wendel HG, Melnick A, Younes A. Emerging epigenetic-modulating therapies in lymphoma. Nat Rev Clin Oncol. 2019;16:494–507.
42. Honma D, Kanno O, Watanabe J, Kinoshita J, Hirasawa M, Nosaka E, et al. Novel orally bioavailable EZH1/2 dual inhibitors with greater antitumor efficacy than an EZH2 selective inhibitor. Cancer Sci. 2017;108:2069–78.
43. Campisi A, Bonfanti R, Raciti G, Bonaventura G, Legnani L, Magro G, et al. Gene silencing of transferrin-1 receptor as a potential therapeutic target for human follicular and anaplastic thyroid cancer. Mol Ther Oncolytics. 2020;16:197–206.
44. Hagag AA, Badraia IM, Abdelmageed MM, Hablas NM, Hazzaa SME, Nosair NA. Prognostic value of transferrin receptor-1 (CD71) expression in acute lymphoblastic leukemia. Endocr Metab Immune Disord Drug Targets. 2018;18:610–7.
45. Callens C, Coulon S, Naudin J, Radford-Weiss I, Boissel N, Raffoux E, et al. Targeting iron homeostasis induces cellular differentiation and synergizes with differentiating agents in acute myeloid leukemia. J Exp Med. 2010;207:731–50.
46. Barabas K, Faulk WP. Transferrin receptors associate with drug resistance in cancer cells. Biochem Biophys Res Commun. 1993;197:702–8.
47. Chitambar CR, Wereley JP. Resistance to the antitumor agent gallium nitrate in human leukemic cells is associated with decreased gallium/iron uptake, increased activity of iron regulatory protein-1, and decreased ferritin production. J Biol Chem. 1997;272:12151–7.
48. Bonnah RA, Hoelter J, Steeghs L, Enns CA, So M, Muckenthaler MU. Lipooligosaccharide-independent alteration of cellular homeostasis in Neisseria meningitidis-infected epithelial cells. Cell Microbiol. 2005;7:869–85.
49. Kenneth NS, Mudie S, Naron S, Rocha S. TfR1 interacts with the IKK complex and is involved in IKK-NF-κB signalling. Biochem J. 2013;449:275–84.
50. Weng J, Chen L, Liu H, Yang XP, Huang L. Ferroptosis markers predict the survival, immune infiltration, and ibrutinib resistance of diffuse large B cell lymphoma. Inflammation. 2022;45:1146–61.
51. Chen D, Chu B, Yang X, Liu Z, Jin Y, Kon N, et al. iPLA2β-mediated lipid detoxification controls p53-driven ferroptosis independent of GPX4. Nat Commun. 2021;12:3644.
52. Yang WS, Stockwell BR. Ferroptosis: death by lipid peroxidation. Trends Cell Biol. 2016;26:165–76.
53. Mizuno H, Kitada K, Nakai K, Sarai A. PrognoScan: a new database for meta-analysis of the prognostic value of genes. BMC Med Genom. 2009;2:18.